

TECHNICAL REPORT

Open Access



Light detection and ranging (LIDAR) laser altimeter for the Martian Moons Exploration (MMX) spacecraft

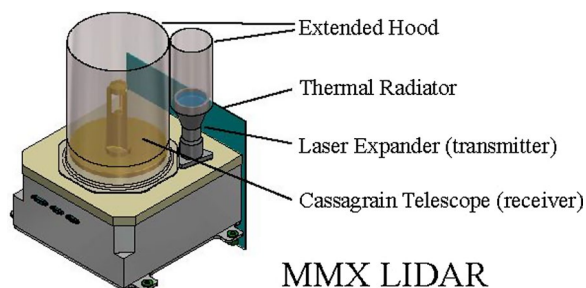
Hiroki Senshu^{1*}, Takahide Mizuno², Kazuhiro Umetani^{3,5}, Toru Nakura⁴, Akihiro Konishi⁵, Akihiko Ogawa^{6,7}, Hirokazu Ikeda², Koji Matsumoto^{8,9}, Hiroto Noda^{8,9}, Yoshiaki Ishihara¹⁰, Sho Sasaki¹¹, Naoki Tateno¹², Yasuyuki Ikuse¹³, Katsunori Mayuzumi¹³, Teiji Kase¹³ and Hisayoshi Kashine¹⁴

Abstract

An altimeter is a critical instrument in planetary missions, for both safe operations and science activities. We present required specifications and link budget calculations for light detection and ranging (LIDAR) onboard the Martian Moons Exploration (MMX) spacecraft. During the mission phase, this LIDAR will continuously measure the distance between the spacecraft and its target. The time-series distance provides important diagnostic information for safe spacecraft operations and important information for geomorphological studies. Because MMX is a sample return mission, its LIDAR must accommodate physical disturbances on the Martian satellite surface. This resulted in changes to the optical system design.

Keywords: LIDAR, MMX, Phobos

Graphical abstract



MMX LIDAR

Introduction

The Martian Moons Exploration (MMX) mission is coordinated by the Japan Aerospace Exploration Agency (JAXA) (Kuramoto et al. 2021). In this mission, a spacecraft will be launched in 2024 and reach Martian orbit in

the following year. After Mars orbit insertion (MOI), the spacecraft will orbit Mars with the same orbital period as Phobos. The spacecraft will appear to be orbiting alongside Phobos, so this is called a quasi-satellite orbit (QSO) (Scheeres 2012; Kuramoto et al. 2021; Nakamura et al. 2021; Matsumoto et al. 2021).

Figure 1 shows a schematic image of QSO in a rotating reference frame centered on Phobos and such that the x-axis is the Mars–Phobos direction. The shape of QSO

*Correspondence: senshu@perc.it-chiba.ac.jp

¹ Planetary Exploration Research Center, Chiba Institute of Technology, 2-17-1 Tsudanuma, Narashino, Chiba 275-0016, Japan

Full list of author information is available at the end of the article

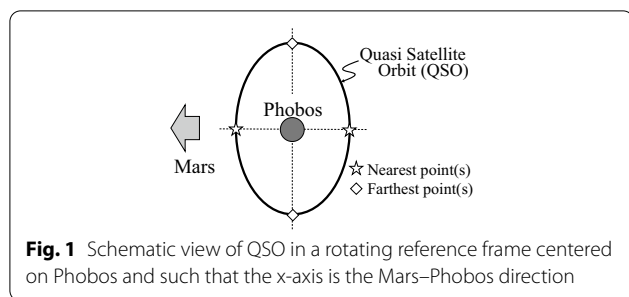


Fig. 1 Schematic view of QSO in a rotating reference frame centered on Phobos and such that the x-axis is the Mars–Phobos direction

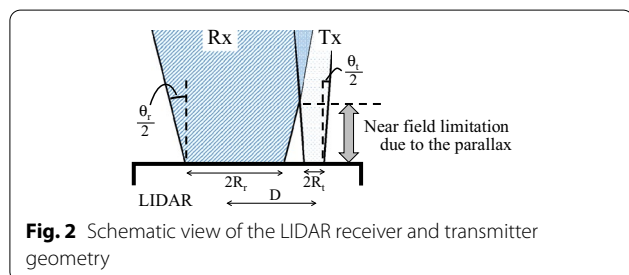


Fig. 2 Schematic view of the LIDAR receiver and transmitter geometry

is not an ellipsoid with Phobos as one foci, but rather a Phobos-centered ellipsoid with an axial ratio of around 1:2. In the Phobos-centered frame, the spacecraft moves fastest at the nearest points and slowest at the farthest points. The nearest points are at the sub-Mars and anti-Mars points and the farthest points are at leading and trailing points. Because Phobos is tidally locked to Mars, the longitudes of sub-nearest and sub-farthest points on Phobos are fixed. Resolutions of observations from QSO are thus determined by the longitude of the target area.

Plans are for MMX to stay near Mars for three earth years. During the mission phase, MMX will land on Phobos up to twice to sample surface materials, which will possibly include Mars-originated material (Kuramoto et al. 2021). The size of QSO changes with mission phases. The highest QSO, named QSO-H, is 100 km × 198 km while the lowest QSO, named QSO-LC, is 20 km × 27 km. Between QSO-H and -LC, middle latitude QSO (QSO-M; 50 km × 94 km) and other low-latitude QSOs (QSO-LA; 30 km × 49 km and LB; 22 km × 31 km) are defined (see Fig. 2 in Nakamura et al. 2021 for more detail). In addition to them, MMX spacecraft approaches Phobos in descent operations such as landing rehearsals, rover deployment, and of course landing operations.

Continuous distance measurements from the satellite to the target, along with taking photographs, are important for safe operations. This information is used to confirm whether operations succeeded and to prepare subsequent operation plans. Continuous measurements along with predicted satellite trajectories and attitude

information acquired from the star-tracker camera determine an arc (a series of LIDAR footprints) in the space. By comparing the predicted arc and the surface morphology of Phobos, the satellite trajectory can be revised with high precision (Matsumoto et al. 2020; Yamamoto et al. 2020). The precise trajectory relative to Phobos is required in data post-processing performed by the other instruments, especially in lower QSO (Nakamura et al. 2021). Continuous distance measurements during decent operations will provide key information related to the density distribution of Phobos. Thus, we developed a light detection and ranging (LIDAR) laser altimeter for MMX. This paper presents specifications and the development status of this LIDAR.

MMX LIDAR

MMX has three laser altimeters, one for scientific observations and two others that are part of the bus system, used during descent operations. This paper focuses on the science-use laser altimeter, called “the LIDAR” below for simplicity. Table 1 summarizes the LIDAR’s specifications. Note that because LIDAR development is still in phase C, these specifications are requirements that the final LIDAR should satisfy. These requirements are derived to meet a mission requirement for LIDAR to obtain the geological structure on Phobos such as fresh and degraded craters and grooves (see also Kuramoto et al. 2021).

The LIDAR is being developed by NEC Corp., who developed the LALT on Kaguya (Araki et al. 2008), the LIDAR on Hayabusa (Mizuno et al. 2010), and the LIDAR on Hayabusa2 (Mizuno et al. 2017). LIDAR development will thus inherit the heritage of these previous laser altimeters. Following Hayabusa2, a passively Q-switched neodymium-doped yttrium aluminum garnet (Nd:YAG) laser is adopted here as the laser transmitter because of its stability against temperature changes (Mizuno et al. 2017). The laser rod is 3φ × 100mm, which is longer than the LIDAR on Hayabusa2 (3φ × 40mm), to achieve laser power exceeding 20mJ. To suppress the beam width, the beam expander magnification was changed from ×3 (Hayabusa2) to ×7 (MMX). The aperture and primary mirror sizes of the Cassegrain telescope in the receiving optics are unchanged from Hayabusa2. The FOV of the Cassegrain is narrower than that of Hayabusa2, which was achieved by rearranging the optics behind the telescope.

The LIDAR on Hayabusa2 had two receiving optics, and active optics were selected according to the target distance, accommodating three orders of magnitude of distance or six orders of magnitude of energy (Mizuno et al. 2017). In contrast, the LIDAR onboard MMX has only one receiving optics (the Cassegrain telescope), but

Table 1 Specifications for LIDAR onboard MMX

Size, weight, energy		
Size	300 × 300 × 360 mm ³	Including hood
Weight	< 4.7 kg	Including tolerance
Energy consumption	< 15 W (nominal)	Excluding heater
Measurement		
Range	100 m–100 km	Assuming target albedo being 0.05
Accuracy	± 2 m @ 100 m	
Frequency	± 22 m @ 100 km	4 Hz at maximum
Receiver		
FOV	1 mrad	Cassegrain-type telescope
Transmitter		
Laser energy	> 20 mJ	Until the end of life
Pulse divergence	< 0.5 mrad	D4σ
Pulse width	< 10 ns (FWHM) < 25 ns (90% energy)	
Energy measurement		
Accuracy	< 10%	For each of receiver and transmitter when the energy of signal > 0.2 fJ

the processing circuit behind the receiver detector (avalanche photodiode; APD) was developed to accommodate an energy range over six orders of magnitude.

LIDARX is a pulse detection IC developed for laser altimeters (Mizuno et al. 2012). It measures pulse timing from a trigger by using a time-to-amplitude converter (TAC), so no high-frequency clock is needed. LIDARX has five channels and four gains for each, allowing dynamic ranges as wide as six orders of magnitude. LIDARX accuracy depends on temperature conditions, so precise calibration data must be acquired before launch.

Link budget calculation

Phobos' surface reflectance is known to locally vary. According to previous observations (e.g., Zellner and Capen 1974; Murchie and Erard 1996; Fraeman et al. 2012) “blue” regions have lower reflectance than the more common “red” regions. Blue regions are observed only inside and around the Stickney crater and thought to comprise primordial materials, and so are of interest in terms of material science and the origin and evolution of Phobos. The morphology of these regions as observed by the LIDAR will thus provide key insights.

The reflectance of blue regions at the Nd:YAG wavelength (1064 nm) is around 0.06 to 0.07 while that of red regions is around 0.08 to 0.09 (Fraeman et al. 2012). In addition to this, the received energy by the LIDAR can change with the slope at the target. Therefore, for safety we adopt $A = 0.05$ as a nominal albedo value

of reflectance in the link budget calculation. Received energy E by APD in LIDAR is

$$E = JA \left(\frac{R}{H} \right)^2 T, \quad (1)$$

where J is the laser pulse energy, R and T are the effective radius and transparency of the receiving optics given in Table 1, respectively, and H is the distance from the target surface. Note that J is not the energy of the laser emitted from the laser rod, but the energy transmitted from the beam expander. Assuming quantum efficiency of 0.4 and an APD multiplication factor of 100, after the LIDAR on Hayabusa2, the charge generation C at APD is

$$C = E \left(\frac{\lambda}{hc} \right)^{-1} \cdot 0.4 \cdot 100e, \quad (2)$$

where λ is the laser wavelength (1064 nm), and h , c , and e are Planck's constant, light speed, and the electron charge, respectively.

To summarize, the expected charge generation per shot is

$$C = 7.04 \times 10^{-15} \times \left(\frac{J}{J_0} \right) \left(\frac{H}{H_0} \right)^{-2}, \quad (3)$$

in unit of coulomb (C), and J_0 and H_0 are given as 20 mJ and 100 km in the equation. Thus, the circuit behind the receiving optics should be able to detect signals as small as $7 \times 10^{-15} C$. This requirement is met by using the LIDARX (Mizuno et al. 2012).

The electric circuit behind the receiver optics was developed to detect pulses while being insensitive to continuous light such as sunshine. However, shot noise caused by continuous light degrades the SNR. Assuming the width of the band-pass filter to be $\Delta\lambda = 5$ nm, solar light radiation to the telescope FOV, J_{\odot} , can be calculated from Plank's law as

$$J_{\odot} = \frac{2hc^2}{\lambda^5} \left(e^{hc/\lambda kT_{\odot}} - 1 \right)^{-1} \cdot \pi R_{\odot}^2 \cdot \Omega \cdot \Delta\lambda, \quad (4)$$

where T_{\odot} and R_{\odot} are the surface temperature and radius of the Sun, respectively, and Ω is the solid angle of the telescope FOV at the target surface from the Sun. This equation gives $J_{\odot} = 14.37\text{kW}$, which is much smaller than the laser light from LIDAR, namely $20\text{ mJ}/10\text{ ns} = 2\text{ MW}$. Fluctuation of scattered solar light is thus negligible in LIDAR observations.

Near-field limitations are not determined by the link budget, but by geometric conditions known as parallax. Figure 2 shows a schematic view of LIDAR's optics. Transmitting and receiving optics are separated by $D = 99.1\text{mm}$, so the nearest target distance H where the receiving FOV contains the entire transmission FOV is

$$H \left(\tan \frac{\theta_r}{2} - \tan \frac{\theta_t}{2} \right) = D - R_r + R_t, \quad (5)$$

where $\theta_r = 1\text{mrad}$ and $\theta_t = 0.5\text{mrad}$ are the receiver and transmitter FOV divergences, respectively, and $R_r = 63.5\text{mm}$ and $R_t = 10.5\text{mm}$ are the receiver and transmitter radii at the base, respectively. Solving this gives $H = 184\text{m}$ as the minimum altitude at which the receiver FOV includes the entire laser footprint.

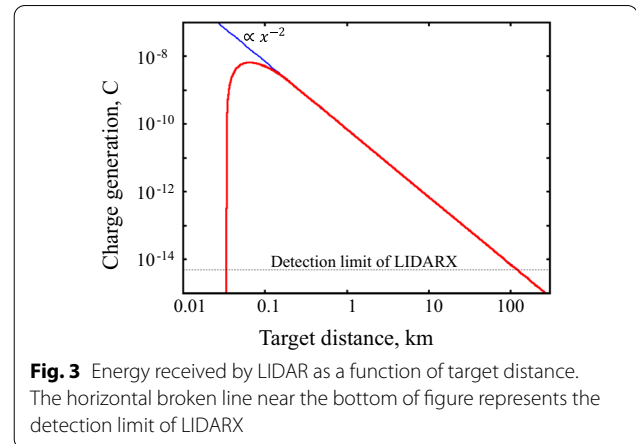
If H satisfies

$$H \left(\tan \frac{\theta_r}{2} + \tan \frac{\theta_t}{2} \right) > D - R_r - R_t, \quad (6)$$

at least part of the transmitting FOV overlaps the receiving FOV. When the distance is 100m , for example, 86% of the transmitter FOV overlaps the receiver FOV. This overlap ratio is sufficient for signal detection, so the LIDAR can measure distances as close as 100m , as required, but the energy distribution in the laser footprint is required to calculate target reflectance. Figure 3 represents the energy received by LIDAR as a function of the target distance taking into account the parallax effect.

Scientific use of LIDAR

The LIDAR continuously measures the distance between MMX and a target at a frequency of 1Hz whenever the LIDAR footprint is on the target. The LIDAR footprint moves westward across Phobos' surface, due to the movement of MMX relative to Phobos, at a speed that depends



on the orbit. The maximum speed of LIDAR footprint on Phobos is attained when MMX is at the nearest point in QSO-LC (8.5m/s). At this time the MMX altitude is around 5.8km , corresponding to a LIDAR footprint size of 2.9m . In this case, therefore, the footprints do not overlap. In QSO-LA, from which landing site candidates are precisely observed (Nakamura et al. 2021, Matsumoto et al. 2021), the maximum footprint speed across the surface is 6.8m/s and the MMX altitude is 16.8km , corresponding to a LIDAR footprint size of 8.4m . In this case, the footprints overlap.

Continuous observations give an east–west cross-sectional morphology along the footprint track. Plans are for MMX to change its attitude northward and southward to image low-latitude regions of Phobos from nominal QSO and mid- and high-latitude regions from 3D-QSO (QSO with inclined orbit plane in Phobos-centered frame for the observation of high-latitude regions; see Nakamura et al. 2021 for more details). The LIDAR footprint will globally cover Phobos by continuous observations simultaneously with global imaging, resulting in a shape model independent of that from camera images. While LIDAR shape model will be at a low lateral resolution than image-based shape model, it should be accurate in terms of altitudes. Especially LIDAR shape model will have an advantage than image-based shape model in sporadic shape such as boulders, gentle slope such as degraded crater walls, and steep wall such as sides of grooves. The LIDAR shape model will thus contribute to improving the global shape model from camera images. Furthermore, comparisons between cross-sectional morphology and camera images will improve estimates of LIDAR alignment (see Noda et al. 2021; for the Hayabusa2 case). Thus, the shape model and LIDAR alignment should be iteratively improved during the MMX mission phase to one or two FOV (Noda et al. 2021).

Observations of surface reflectance from various incident angles provide roughness information at smaller scales than the footprint. If the target surface is flat, the phase function is given as a simple cosine function. On the other hand, when the target surface is rough, the bulk phase function of the surface is given by the superposition of phase functions for each small region with various angles in the surface of interest. As a result the bulk phase function deviates from the original cosine function with roughness (Yamada et al. 2017). Thus, the comparison between the cosine function and the phase function obtained by LIDAR gives the information on the roughness within the LIDAR footprint.

In north–south scanning observations, the footprint moves faster than in stable nadir observations. LIDAR observations occur at frequencies exceeding 1Hz, but are limited to short durations (approximately 1min) due to thermal restrictions. We therefore need a strategy for performing high-frequency observations, but this strategy will be discussed through LIDAR development and operations to maintain flexibility.

The distance from Phobos changes by around a factor of two during each orbital period (Kuramoto et al. 2021; Nakamura et al. 2021). The receiver circuit gain should be arranged in detail to optimize reflectance measurements. As described above, LIDARX has five channels with four gains for each, 20 combinations in total. The LIDAR will have an auto gain control (AGC) function by which the optimum channel-and-gain combination is selected according to the previously acquired range and energy. The details of changing channel/gain combinations will be determined through performance testing of the flight model.

Hood extension

MMX is a sample return mission from a Martian moon, so plans are for landing on Phobos up to twice. Thrusters might disturb the surface during decent and ascent operations, and surface materials will be ejected from footpads at landing and from sampling sites during sampling operations. These materials or dust may damage or impede the LIDAR transmitting and receiving optics.

Reviewing the positions of possible dust sources, we found the lateral distance to the nearest dust source to be 638mm. We decided to extend the hood of the receiving telescope so that surface dust grains will not directly hit the LIDAR's primary telescope mirror (see Fig. 4). The primary mirror is supposed to be separated from the surface by 885mm when MMX is on the surface. Thus, to protect the primary mirror from direct dust impacts, the ϕ 137mm telescope hood length should exceed 172mm in front of the primary mirror. Because the primary mirror is separated from the hood base plate by 22mm, the hood

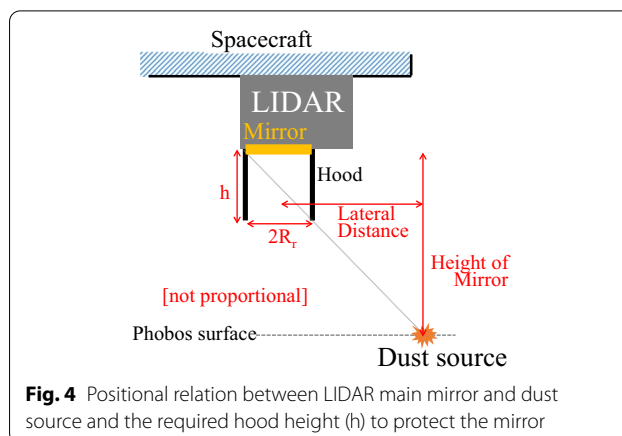


Fig. 4 Positional relation between LIDAR main mirror and dust source and the required hood height (h) to protect the mirror

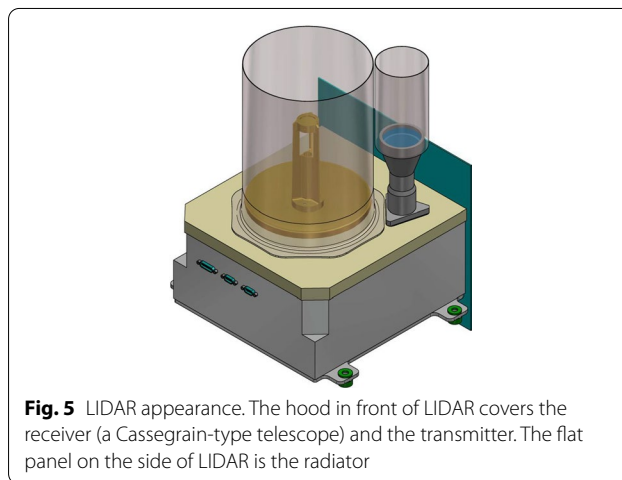


Fig. 5 LIDAR appearance. The hood in front of LIDAR covers the receiver (a Cassegrain-type telescope) and the transmitter. The flat panel on the side of LIDAR is the radiator

length should exceed 194mm in total, which is 70mm longer than the Hayabusa2 hood (124mm). The transmitter optics (expander) are also to be protected from dust, so we also place a hood in front of the expander and the transmitter hoods, molded integrally with the telescope hood. Figure 5 shows the appearance with the extended hood. This hood extension does not affect the link budget, because the transmitting and receiving FOVs are both sufficiently narrow. Thermal and vibrational conditions are satisfied even with the extended hood.

Summary

We are developing a laser altimeter (LIDAR) for MMX. The LIDAR satisfies requirements for measuring the distance between the satellite and Phobos from altitudes of 100 m to 100 km by using a pulse detection IC named LIDARX. The LIDAR data will be used not only to clarify the global scale surface structure of Phobos, but also to provide diagnostic information on the local scale surface roughness. By comparison between continuous LIDAR data and a Phobos shape model, we can improve the orbit

of spacecraft. LIDAR will not operate at below 100 m, but we should prepare for preventing physical damage from surface material ejected from footpads during landing operation. Thus we decided to expand both of Tx and Rx hoods. LIDAR development is proceeding on schedule for mounting on MMX, which will be launched in 2024.

Acknowledgements

We thank Mr. Daichi Tokiwa and Mr. Yusuke Aonuma for their help in basic experiments on LIDARX.

Authors' contributions

Design of the work: HS. Manuscript preparation: HS, TM, KM, and YI. Figure preparation: HS, TK, and HK. All authors read and approved the final manuscript.

Funding

Not applicable.

Availability of data and materials

The datasets used and/or analyzed during the current study are available from the corresponding author on reasonable request.

Declarations

Competing interests

The authors declare that they have no competing interests.

Author details

¹Planetary Exploration Research Center, Chiba Institute of Technology, 2-17-1 Tsudanuma, Narashino, Chiba 275-0016, Japan. ²Department of Spacecraft Engineering, Institute of Space and Astronautical Science, Japan Aerospace Exploration Agency, 3-1-1 Yoshinodai, Chuo-ku, Sagami-hara, Kanagawa 252-5210, Japan. ³Graduate School of Engineering, Tohoku University, Aramaki Aza-Aoba 6-6, Sendai, Miyagi 980-8579, Japan. ⁴Department of Electronics Engineering and Computer Science, Fukuoka University, 8-19-1 Nanakuma, Jonan-ku, Fukuoka 814-0180, Japan. ⁵Present Address: Graduate School of Natural Science and Technology, Okayama University, 3-1-1, Tsushimanaka, Kita-ku, Okayama 700-8530, Japan. ⁶Department of Mechanical Engineering, Graduate School of Engineering, Tokai University, 4-1-1 Kitakinme, Hiratsuka-cho, Kanagawa 259-1292, Japan. ⁷Present Address: IHI Aero Space Company Limited, Tokyo, Japan. ⁸National Astronomical Observatory of Japan, 2-12 Hoshigaoka, Mizusawa, Oshu, Iwate 023-0861, Japan. ⁹The Graduate University for Advanced Studies, SOKENDAI, Shonan Village, Hayama, Kanagawa 240-0193, Japan. ¹⁰JAXA Space Exploration Center (JSEC), Japan Aerospace Exploration Agency, 3-1-1 Yoshinodai, Chuo-ku, Sagami-hara, Kanagawa 252-5210, Japan. ¹¹Department of Earth and Space Science, Osaka University, 1-1 Machikaneyama-cho, Toyonaka, Osaka 560-0043, Japan. ¹²Space Utilization Promotion Department, Japan Space Forum, 3-2-1 Kandasurugadai, Chiyoda-ku, Tokyo 101-0062, Japan. ¹³NEC Corp., 1-10 Nisshin-cho, Fuchu City, Tokyo 183-8501, Japan. ¹⁴NEC Platforms, Ltd., 5-22-5 Sumiyoshi-cho, Fuchu City, Tokyo 183-8502, Japan.

Received: 15 January 2021 Accepted: 24 October 2021

Published online: 14 December 2021

References

- Araki H, Tazawa S, Noda H, Tsubokawa T, Kawano N, Sasaki S (2008) Observation of the lunar topography by the laser altimeter LALT on board Japanese lunar explorer SELENE. *Adv Space Res* 42(2):317–322. <https://doi.org/10.1016/j.asr.2007.05.042>
- Fraeman AA, Arvidson RE, Murchie SL, Rivkin A, Bibring JP, Choo TH, Gondet B, Humm D, Kuzmin RO, Manaud N, Zabalueva EV (2012) Analysis of disk-resolved OMEGA and CRISM spectral observations of Phobos and Deimos. *J Geophys Res* 117:E00J15. <https://doi.org/10.1029/2012JE004137>

- Kuramoto K, Kawakatsu Y, Fujimoto M, Barucci MA, Lawrence DJ, Genda H, Hirata N, Imamura T, Kameda S, Kobayashi M, Kusano H, Matsumoto K, Michel P, Miyamoto H, Nakagawa H, Nakamura T, Ogawa K, Otake H, Ozaki M, Russel S, Sasaki S, Sawada H, Senshu H, Terada N, Ulamec S, Usui T, Wada K, Yokota S (2021) Martian Moons Exploration MMX: Sample return mission to Phobos elucidating formation processes of habitable planets. *Earth Planets Space*. <https://doi.org/10.1186/s40623-021-01545-7>
- Matsumoto K, Noda H, Ishihara Y, Senshu H, Yamamoto K, Hirata N, Hirata N, Namiki N, Otsubo T, Higuchi A, Watanabe S, Ikeda H, Mizuno T, Yamada R, Araki H, Abe S, Yoshida F, Sasaki S, Oshigami S, Tsuruta S, Asari K, Shizugami M, Yamamoto Y, Ogawa N, Kikuchi S, Saiki T, Tsuda Y, Yoshikawa M, Tanaka S, Terui F, Nakazawa S, Yamaguchi T, Takei Y, Takeuchi H, Okada T, Yamada M, Shimaki Y, Shirai K, Ogawa K, Iijima Y (2020) Improving Hayabusa2 trajectory by combining LIDAR data and a shape model. *Icarus* 338:113574. <https://doi.org/10.1016/j.icarus.2019.113574>
- Matsumoto K, Hirata N, Ikeda H, Kouyama T, Senshu H, Yamamoto K, Noda H, Miyamoto H, Araya A, Araki H, Kamata S, Namiki N (2021) MMX geodesy: science and observation strategy. *Earth Planets Space*. <https://doi.org/10.1186/s40623-021-01500-6>
- Mizuno T, Tsuno K, Okumura E, Nakayama M (2010) Evaluation of LIDAR System in Rendezvous and Touchdown Sequence of Hayabusa Mission. *Trans Japan Soc Aero Space Sci* 53(179):47–53
- Mizuno T, Kase T, Shiina T, Mita M, Namiki N, Senshu H, Yamada R, Noda H, Kunimori H, Hirata N, Terui F, Mimasu Y (2017) Development of the Laser Altimeter (LIDAR) for Hayabusa2. *Space Sci Rev* 208:33–47. <https://doi.org/10.1007/s11214-015-0231-2>
- Mizuno T, Ikeda H, Kawahara K (2012) Pulse detection IC for a laser altimeter using CMOS technology. *Trans JSASS Aerospace Tech Jpn* 10(28):Pd_101-Pd_105
- Murchie S, Erard S (1996) Spectral properties and heterogeneity of Phobos from measurements by Phobos 2. *Icarus* 123:63–86
- Nakamura T, Ikeda H, Kouyama T, Nakagawa H, Kusano H, Senshu H, Kameda S, Matsumoto K, Takeo Y, Baresi N, Oki Y, Lawrence DJ, Chabot N, Peplowski P, Antonietta BM, Eric S, Yokota S, Terada N, Ulamec S, Patrick M, Kobayashi M, Hirata N, Wada K, Miyamoto H, Imamura T, Ogawa N, Ogawa K, Iwata T, Imada T, Otake H, Canalias E, Lorda L, Elisabet C, Tardivel S, Mary S, Kunugi M, Mitsuhashi S, Merlin F, Fornasier S, Rees J-M, Bernardi P, Imai S, Ito Y, Ishida H, Kuramoto K, Kawakatsu Y (2021) Science operation plan of Phobos and Deimos from the MMX spacecraft. *Earth Planets Space*. <https://doi.org/10.1186/s40623-021-01546-6>
- Noda H, Senshu H, Matsumoto K, Namiki N, Mizuno T, Seiji S, Abe S, Araki H, Asari K, Cho Y, Fujii A, Hayakawa M, Higuchi A, Hirata N, Hirata N, Honda C, Honda R, Ishihara Y, Kameda S, Kikuchi S, Kouyama T, Matsuoka M, Mimasu Y, Morota T, Nakazawa S, Ogawa K, Ogawa N, Ono G, Oshigami S, Saiki T, Sakatani N, Sasaki S, Sawada H, Shizugami M, Suzuki H, Takahashi T, Takei Y, Tanaka S, Tatsumi E, Terui F, Tsuda Y, Tsuruta S, Watanabe S, Yamada M, Yamada R, Yamaguchi T, Yamamoto K, Yokota Y, Yoshida F, Yoshikawa K, Yoshikawa M, Yoshioka K (2021) Alignment determination of the Hayabusa2 laser altimeter (LIDAR). *Earth Planets Space*. <https://doi.org/10.1186/s40623-020-01342-8>
- Scheeres DJ (2012) *Orbital Motion in Strongly Perturbed Environments*. Springer. ISBN 978-3-642-03256-1
- Yamada R, Senshu H, Namiki N, Mizuno T, Abe S, Yoshida F, Noda H, Hirata N, Oshigami S, Araki H, Ishihara Y, Matsumoto K (2017) Albedo Observation by Hayabusa2 LIDAR: Instrument Performance and Error Evaluation. *Space Sci Rev* 208:49–64. <https://doi.org/10.1007/s11214-016-0240-9>
- Yamamoto K, Otsubo T, Matsumoto K, Noda H, Namiki N, Takeuchi H, Ikeda H, Yoshikawa M, Yamamoto Y, Senshu H, Mizuno T, Hirata N, Yamada R, Ishihara Y, Araki H, Abe S, Yoshida F, Higuchi A, Sasaki S, Oshigami S, Tsuruta S, Asari K, Shizugami M, Ogawa N, Ono G, Mimasu Y, Yoshikawa K, Takahashi T, Takei Y, Fujii A, Yamaguchi T, Kikuchi S, Watanabe S, Tanaka S, Terui F, Nakazawa S, Saiki T, Tsuda Y (2020) Dynamic precise orbit determination of Hayabusa2 using laser altimeter (LIDAR) and image tracking data sets. *Earth Planets Space* 72:85. <https://doi.org/10.1186/s40623-020-01213-2>
- Zellner BH, Capen RC (1974) Photometric properties of the Martian satellites. *Icarus* 23(3):437–444

Publisher's Note

Springer Nature remains neutral with regard to jurisdictional claims in published maps and institutional affiliations.